Research Papers

GREENSUSMATER

Greensusmater
Vol. 3, No. 2, 2026
https://doi.org/10.62755/gsm.2026.07

Check for updates

Comparative Study on Cu(II) and Pb(II) Removal from Water Using $MnFe_2O_4$ and $MnFe_2O_4$/Zeolite Hybrid Adsorbents

Ramlan Ramlan[1,*], Luh Ayu Melinia[1], Endah Puspita[1], Marzuki Naibaho[1,2,3], Akmal Johan[1], Akhmad Aminuddin Bama[1], Masno Ginting[3]

[1] *Department of Physics, Faculty of Mathematics and Natural Science, Universitas Sriwijaya, Inderalaya, Ogan Ilir (OI) 30662, Indonesia*
[2] *Department of Physics, Faculty of Mathematics and Natural Science, Universitas Indonesia, Depok 16424, Indonesia*
[3] *Research Center for Energy Materials (PRME) – National Research and Innovation Agency (BRIN), Complex Puspiptek Building 440-441, Tangerang-South, Banten 15314, Indonesia*

Corresponding author: ramlan@unsri.ac.id

ARTICLE HISTORY: Received: April 2, 2026 | Revised: May 26, 2026 | Accepted: June 8, 2026

ABSTRACT

$MnFe_2O_4$ and $MnFe_2O_4$-Zeolite have been synthesized from sand and zeolite using the co-precipitation method for absorbing ions Pb(II) and Cu(II) in aqueous media. Samples were then characterized using SEM-EDX, XRD, VSM, BET, and AAS. The results of SEM-EDX show that the particle shape of $MnFe_2O_4$ and $MnFe_2O_4$-Zeolite is not uniform. $MnFe_2O_4$ particle size is 5-25 µm, and $MnFe_2O_4$-zeolite 2-29 µm, and there are impurities such as Mg, Cl, Ti, and V. XRD results confirm the presence of $MnFe_2O_4$ and other phases such as TiO_2 and SiO_2. VSM measurement shows that both $MnFe_2O_4$ and $MnFe_2O_4$-Zeolite are soft magnets with coercivity values of 302.12 and 406.04 Oe respectively. While BET analysis shows that the surface area, pore volume, and pore size of $MnFe_2O_4$-zeolite are 222.91 m^2/g, 0.30 cm^3/g, and 2.70 nm, respectively, larger than those of $MnFe_2O_4$. Then, the AAS measurement shows the optimum adsorption for Pb and Cu ions using $MnFe_2O_4$ at a dose of 100 mg/L are 96.59% and 99.24%, while for the $MnFe_2O_4$–zeolite adsorbent for Pb ion at a dose of 100 mg/L is 96.91% and for Cu ion at a dose of 50 mg/L is 99.54%. In general, it was found that the adsorption percentage for both Pb and Cu ions was higher using the $MnFe_2O_4$–zeolite than the $MnFe_2O_4$.

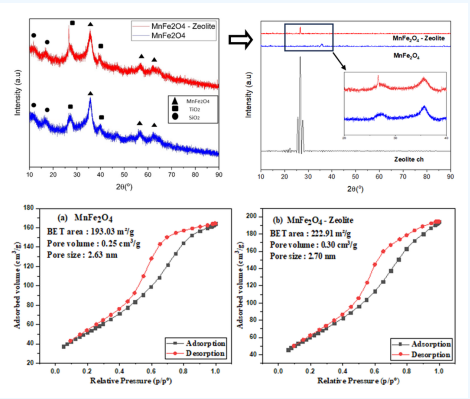

Keywords: *Co-Precipitation; MnFe2O4-Zeolite; Adsorbents; Pb(II) Removal; Cu(II) Removal; Heavy Metal Adsorption*

1. INTRODUCTION

Lead (Pb) and copper (Cu) are known as toxic heavy metals that pose serious risks to human health. Even at low concentrations, lead exposure can damage vital organs such as the kidneys, liver, and reproductive system, while excessive copper intake may cause gastrointestinal disorders and, in severe cases, death [1,2,3,4,5]. Given the negative impact caused by waste metal ions Pb and Cu, it is important to purify water to remove contaminants from Pb and Cu ions [6]. Various conventional techniques can be carried out, such as reverse osmosis [7], ion exchange [8], chemical precipitation [9], solvent extraction [10], etc. The adsorption method is the most appropriate method for removing heavy metal ions from water, with high effectiveness and economy [11].

Several adsorbents have been used to adsorb heavy metal ions from aqueous solutions; namely, sawdust of eucalyptus, dates, and limes [12], $\alpha-Fe_3O_4$ nanoparticles [13,14,15], membrane [16], carbon [17], bentonite [18], zeolite [19][20], manganese ferrite [21], zinc ferrite [22], manganese ferrite-biochar [23] and bentonite-manganese ferrite [24]. Some of these adsorbents have disadvantages such as low adsorption and difficulty in separating from the solution [25]. With the development of research on advanced materials on water pollution by heavy metals, research on manganese ferrite ($MnFe_2O_4$) adsorbents continues to grow every year. $MnFe_2O_4$ adsorbent can be used to remove heavy metal ions with magnetic separation from the solution [26]. However, the $MnFe_2O_4$ adsorbent is easily agglomerated in the liquid phase, reducing the surface area and lowering the adsorption capacity. Zeolite has a larger surface area, more active sites, and high porosity, which can increase the adsorption efficiency [27]. Thus, this study reports the synthesis of $MnFe_2O_4$ and $MnFe_2O_4$–zeolite from natural iron sand using the co-precipitation method [28,29,30,31], along with the evaluation of their ability to adsorb Pb(II) and Cu(II) ions from aqueous solution.

2. EXPERIMENTAL SECTION

2.1 Materials

The materials used in this study were 200 mesh natural iron sand, 32% HCl (Merck), 25% NH_4OH (Technical), $MnCl_2$ 98% (Merck), Zeolite Clinoptilolite from PT. Sari Mas in Medan (Indonesia), Ethanol 96% (Technical), and NaOH 98% (Technical).

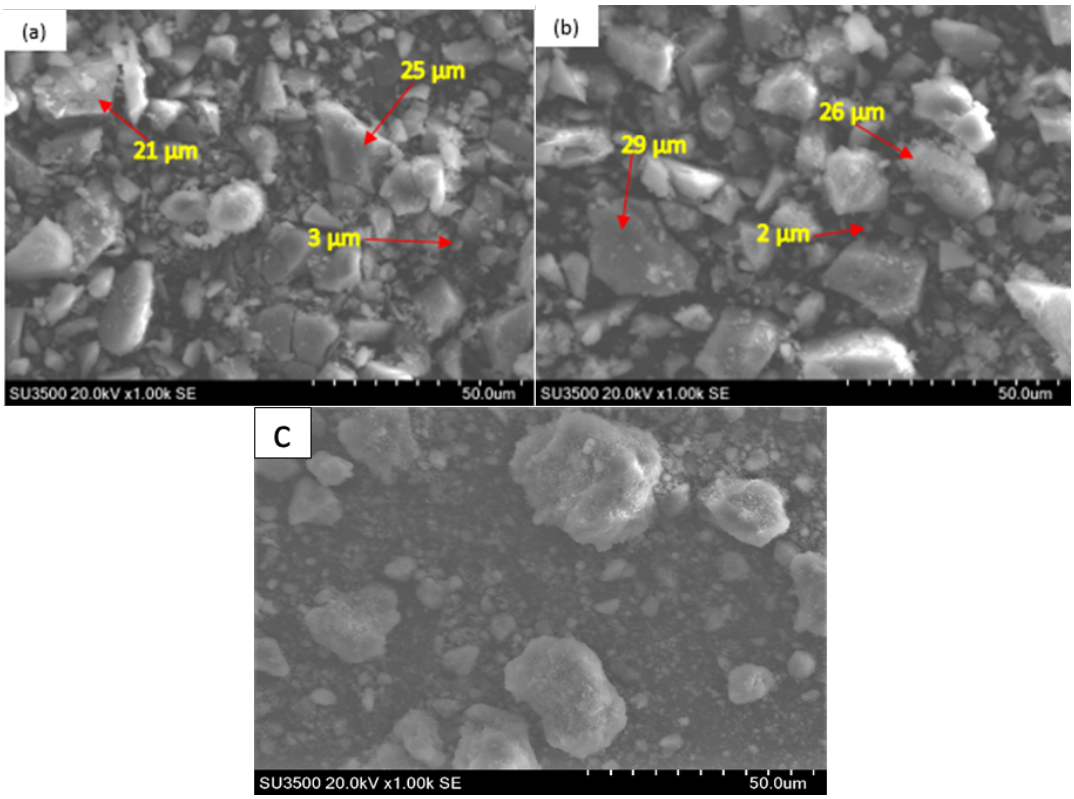

Figure 1. Surface morphology of adsorbents a) $MnFe_2O_4$, and b) $MnFe_2O_4$–zeolite, c) Zeolite.

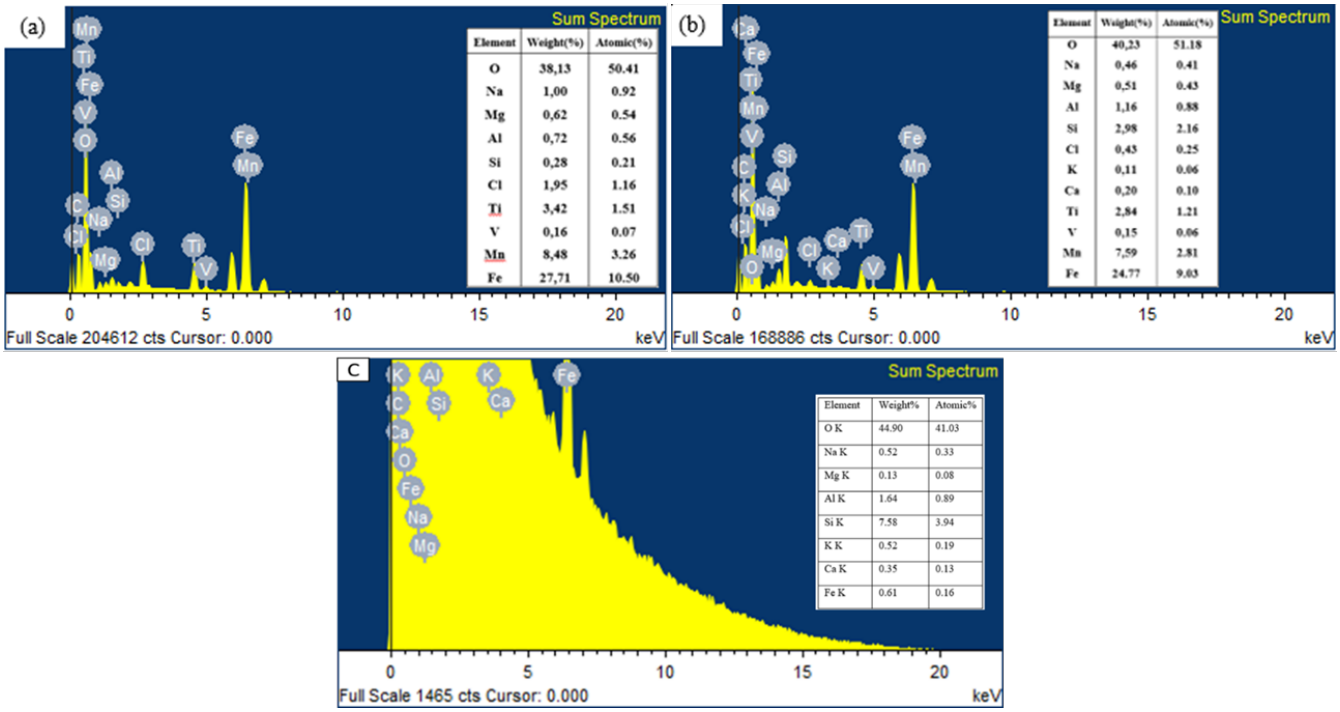

Figure 2. Elemental content of adsorbents a) $MnFe_2O_4$, and b) $MnFe_2O_4$–Zeolite, c) Zeolite.

2.2 Methods

In this study, the synthesis of $MnFe_2O_4$ and $MnFe_2O_4$–zeolite has been done using the co-precipitation method. The co-precipitation method has a simple process and can produce particles that are very small grain size and tend to be more uniform. However, the coprecipitation method will not be able to remove impurities completely. $MnCl_2$, iron sand, and clinoptilolite zeolite were used as the main precursors. Iron sand that has passed 200 mesh is dissolved using 17 ml of HCl and stirred at 500 rpm for 30 minutes at 80 °C, then filtered using Whatman filter paper (Grade 40 Circles). The iron sand filtrate was then mixed with $MnCl_2$ solution at a

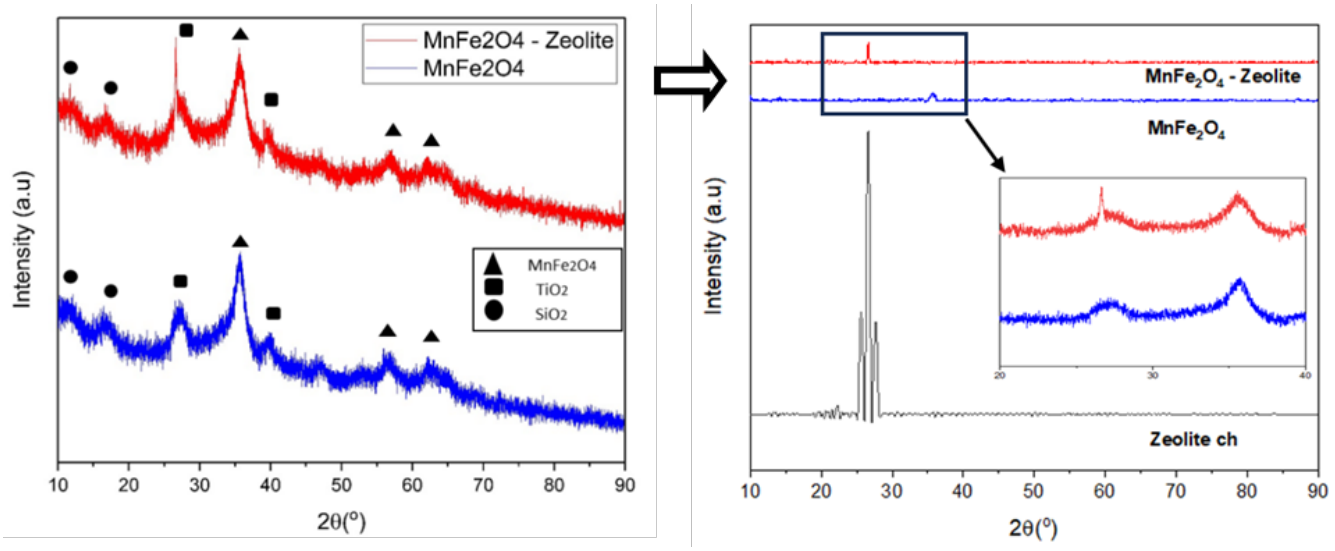

Figure 3. The pattern of diffraction peaks in $MnFe_2O_4$ and $MnFe_2O_4$–zeolite samples.

ratio of 2:1 volume. Furthermore, stirring was carried out with a magnetic bar at 500 rpm at room temperature until the solution became homogeneous. $MnFe_2O_4$–zeolite was made by adding 1 gram of zeolite to the solution, followed by stirring for 40 minutes at 500 rpm at room temperature. Next, the temperature of the solution was changed to 70°C before adding sodium hydroxide solution (5 mol/L) to adjust the solution pH value to 11, after which the resulting solution was stirred for 1 hour. The precipitated composite was then dried in an oven at 100°C for 24 hours. The composite was then crushed using a mortar and was ready to be used as an adsorbent. Next, prepare the following parameters (pH = 5, T = 25 °C, t = 60 minutes, Ci = 8 mg/L) in the form of a solution and put the absorbent into the next batch absorption test.

2.3 Characterization

The samples were then characterized using X-ray diffraction (XRD, SmartLab Rigaku) and Scanning Electron Microscopes (SEM-EDX, Hitachi SU-3500), Brunauer Emmett-Teller (BET, Micrometrics ASAP 2020, USA), and room temperature hysteresis loop measured by Vibrating Sample Magnetometer (VSM 250). In the batch adsorption process using a shaker carried out at optimum conditions (pH=5, T = 25 °C, t = 60 minutes, Ci= 8 mg/L)[24], [32] and the results will be tested using Atomic Absorption Spectrometry (AAS Agilent Technologies-200 series AAA/240 FS AA).

3. RESULT AND DISCUSSION

3.1 Adsorbent Characterization

The surface morphology of $MnFe_2O_4$ and $MnFe_2O_4$–zeolite adsorbents obtained from SEM-EDX measurements are shown in Figure 1. Figure 1a shows that the shape of the $MnFe_2O_4$ particles is not uniform, the surface is still not uniform. The non-uniformity of the particle shape is indicated by the size range of the $MnFe_2O_4$ adsorbent particles from 3 µm to 25 µm. Particles with a large size (21 µm) experience agglomeration, because natural interactions occur between magnetic particles, causing several agglomerated areas [33]. Figure 1b shows the $MnFe_2O_4$–zeolite adsorbent also having a non-uniform particle shape and size. The particle size range of the $MnFe_2O_4$–zeolite adsorbents is 2 µm to 29 µm. It seems that, on average, the particle size of $MnFe_2O_4$-zeolite is larger than that of $MnFe_2O_4$. Meanwhile, in Figure 1c is the morphology of zeolite with a magnification of 1000, we can see that zeolite is agglomerated. The zeolite exhibits an irregular surface morphology with no distinct surface pores, which can be attributed to the coverage of pores by adsorbed organic impurities, surface oxides, and water molecules trapped within the zeolite structure.

The elemental content of $MnFe_2O_4$ and $MnFe_2O_4$–zeolite adsorbents that are also obtained from SEM-EDX measurements is shown in Figure 2. Figure 2a shows that the $MnFe_2O_4$ adsorbent has several elements such as O, Na, Mg, Al (0.72%), Si (0.28%), Cl, Ti, V, Mn, and Fe. All these elements are mostly found in all iron sands with different percentages. The highest percentage of elemental content was in the elements O, Fe, and Mn which are 38.13%, 27.71%, and 8.48%, respectively which confirmed the formation of the $MnFe_2O_4$ compound. Whereas Figure 2b shows that the content of Fe (24.77%) and Mn (7.59%) elements decreased, but the content of Al (1.16%) and Si (2.98%) increased. This is due to the presence of Al and Si content in the zeolite. Other elements present in the $MnFe_2O_4$–zeolite adsorbent are Na, Mg, Cl, K, Ca, Ti, and V. The elements Na, K, and Ca are cations from zeolite, while the presence of elements Mg, and Ti are predicted to appear from the sand that was used, while Cl probably appears from the use of the HCl solvent during the synthesis process. Element V is thought to have originated from the iron sand milling process which experienced abrasion in the jar mill or ball mill.

Figure 3 shows the XRD spectra for $MnFe_2O_4$ and $MnFe_2O_4$–zeolite. It can be seen that $MnFe_2O_4$ adsorbent has several diffraction peaks with different intensities. The highest diffraction peak and several other peaks were identified as phases at values 2θ = 35.57°, 46.82°, 56.76°, and 62.13° with hkl planes (311), (331), (511), and (440) which were matched with JCPDS data No. 73-1964 [34]. At 2θ values of 27.40° and 39.80° TiO_2 compounds were identified, while at 2θ values of 12.22° and 16.39° SiO_2 compounds were identified. The formation of TiO_2 (from iron sand) and SiO_2 (from zeolite) can be seen from the presence of Ti, Si, and O elements in the sample as shown in the EDX analysis. Furthermore, in the

Table 1. The adsorption capacity of Pb and Cu ions by $MnFe_2O_4$ and $MnFe_2O_4$–Zeolite adsorbents.

Dose (mg)	pH	Time (min)	$MnFe_2O_4$						$MnFe_2O_4$–Zeolite					
			Conc. (mg/L)				Cap. (mg/g)		Conc. (mg/L)				Cap. (mg/g)	
			Pb		Cu		Pb	Cu	Pb		Cu		Pb	Cu
			C_i	C_e	C_i	C_e			C_i	C_e	C_i	C_e		
50	5	60	8	0.276	8	0.061	2.57	2.44	8	0.248	8	0.037	2.58	2.65
100	5	60	8	0.273	8	0.064	3.86	3.97	8	0.261	8	0.040	3.88	3.98
150	5	60	8	0.282	8	0.069	7.72	7.94	8	0.263	8	0.047	7.74	7.96

XRD diffraction pattern of the $MnFe_2O_4$–zeolite adsorbent, several peaks were also observed at 2θ values, they are at 12.74°, 16.37°, 20.86°, 26.57°, 35.61°, 39,46°,47, 00°, 56.88°, and 62.00°. In the analysis results, new phases appear at values of 2θ 12.74°, 16.37°, 20.86°, and 26.57°, which were analyzed zeolite compounds (Hydrous sodium aluminum silicate) that were matched with JCPDS data No. 00-019-1180 [35]. Analcime zeolite has the smallest pores and exhibits a compact structure. Compared to other zeolites with ideal unit cells $Na16[(AlO_2)16(SiO_2)32].16H_2O$ [36].

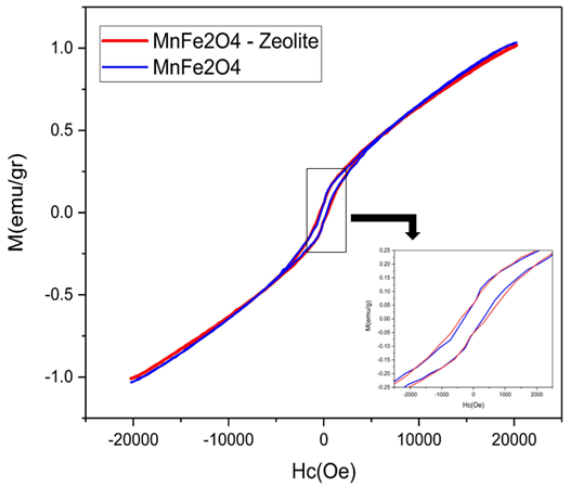

Figure 4. Hysteresis curves of adsorbents for $MnFe_2O_4$ and $MnFe_2O_4$–zeolite.

Furthermore, Figure 4 presents hysteresis curves from VSM measurements for both $MnFe_2O_4$ and $MnFe_2O_4$–zeolite composites. The loop shapes confirm that both samples are ferrimagnetic and can be classified as soft magnetic materials [37]. The pure $MnFe_2O_4$ sample exhibits a saturation magnetization (Ms) of 1.03 emu/g, remanent magnetization (Mr) of 0.05 emu/g, and coercivity (Hc) of 302.12 Oe. In contrast, the $MnFe_2O_4$–zeolite composite shows Ms = 1.02 emu/g, Mr = 0.06 emu/g, and Hc = 406.04 Oe. The slight reduction in Ms in the composite is attributed to the dilution by non-magnetic zeolite phases [38]. The low absolute values of Ms, Mr, and Hc for both samples are likely influenced by the presence of gangue or impurity phases, as evidenced by EDX and XRD analyses [39].

The adsorption-desorption isotherms of N2 from $MnFe_2O_4$ and $MnFe_2O_4$–zeolite samples results that are obtained from the BET measurement, are shown in Figure 5. The N2 adsorption-desorption isotherms of the two adsorbents, including the type V isotherm with the H2 hysteresis loop between the adsorption and desorption curves at higher relative pressures, which shows a mesoporous surface with a complex pore structure interconnected with different sizes [40][41]. The mesoporous surface is evidenced by the pore size of the $MnFe_2O_4$ and $MnFe_2O_4$–zeolite adsorbents, which are 2.63 nm and 2.70 nm. Differences in the shape and size of pores are caused by non-uniform particle size and shape, as shown by the SEM analysis. Calculation of the specific surface area of $MnFe_2O_4$–zeolite (222.91 m^2/g) is much larger than that of $MnFe_2O_4$ (193.03 m^2/g). Besides that, the pore volume of $MnFe_2O_4$–zeolite (0.30 cm3/g) is larger than that of the $MnFe_2O_4$ adsorbent (0.25 cm^3/g). This is clearly due to zeolite being a material that has a high specific surface area and high porosity [42].

3.2 Adsorption of Pb and Cu

The Adsorption capacity of Pb and Cu ions by $MnFe_2O_4$ and $MnFe_2O_4$–zeolite adsorbents is shown in Table 1. The adsorption capacity and removal efficiency are obtained using:

$$q = \frac{(C_i - C_e)\ V}{W} \quad (1)$$

$$R = \frac{(C_i - C_e)}{C_i} \times 100\% \quad (2)$$

with: q = Adsorption capacity (mg/g), Ci = initial concentration (mg/L), Ce = Final concentration (mg/L), V= volume of adsorbate solution (L), W = mass of magnetic powder (g), R = Removal Efficiency (%).

As can be seen from Table 1 for $MnFe_2O_4$ the optimum adsorption capacity values were obtained at a dose of 50 mg/L for both Pb (7.72 mg/g) and Cu (7.94 mg/g) respectively. For $MnFe_2O_4$–zeolite, the optimum adsorption capacity was also observed at a dose of 50 mg/L for Pb (7.74 mg/g) and Cu (7.96 mg/g). The adsorption capacity decreased by increasing the dose in both absorbents. This is predicted due to all the active sites are completely exposed at lower doses, whereas only a small proportion of active sites are exposed at higher doses. Thus, higher adsorbent doses can cause aggregation, which decreases the total surface area of the adsorbent and causes a decrease in adsorption [43]. Another possibility could be caused by the unsaturation of adsorption sites through adsorption reactions [44].

The optimum adsorption capacity value obtained for $MnFe_2O_4$–zeolite adsorbent is slightly larger compared to the $MnFe_2O_4$ adsorbent for both Pb and Cu. This is due to the addition of zeolite to the adsorbent which increases the surface area, pore volume, and pore size thereby increasing the number of active sites on the surface, which can increase the adsorption capacity [27].

The removal efficiency of Pb(II) and Cu(II) metal ions for $MnFe_2O_4$ and $MnFe_2O_4$-Zeolite adsorbents at pH=5, T=25 °C, t= 60 minutes, Ci= 8mg/L is shown in Figure 6. From

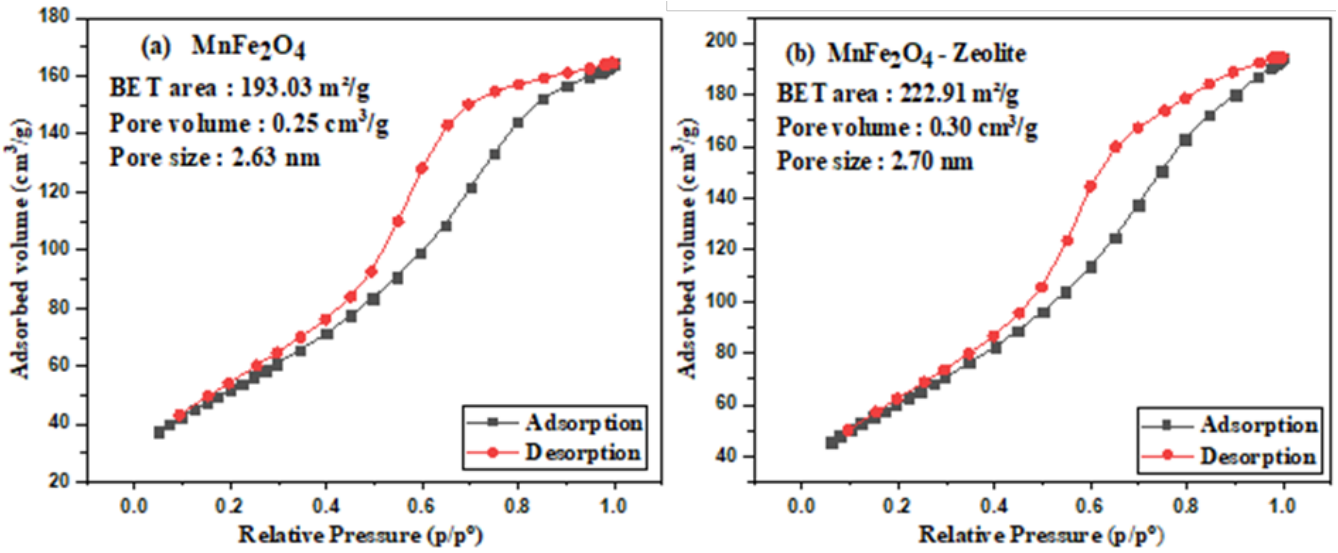

Figure 5. Adsorption-desorption isotherms of N2 from adsorbents a) $MnFe_2O_4$, and b) $MnFe_2O_4$–zeolite.

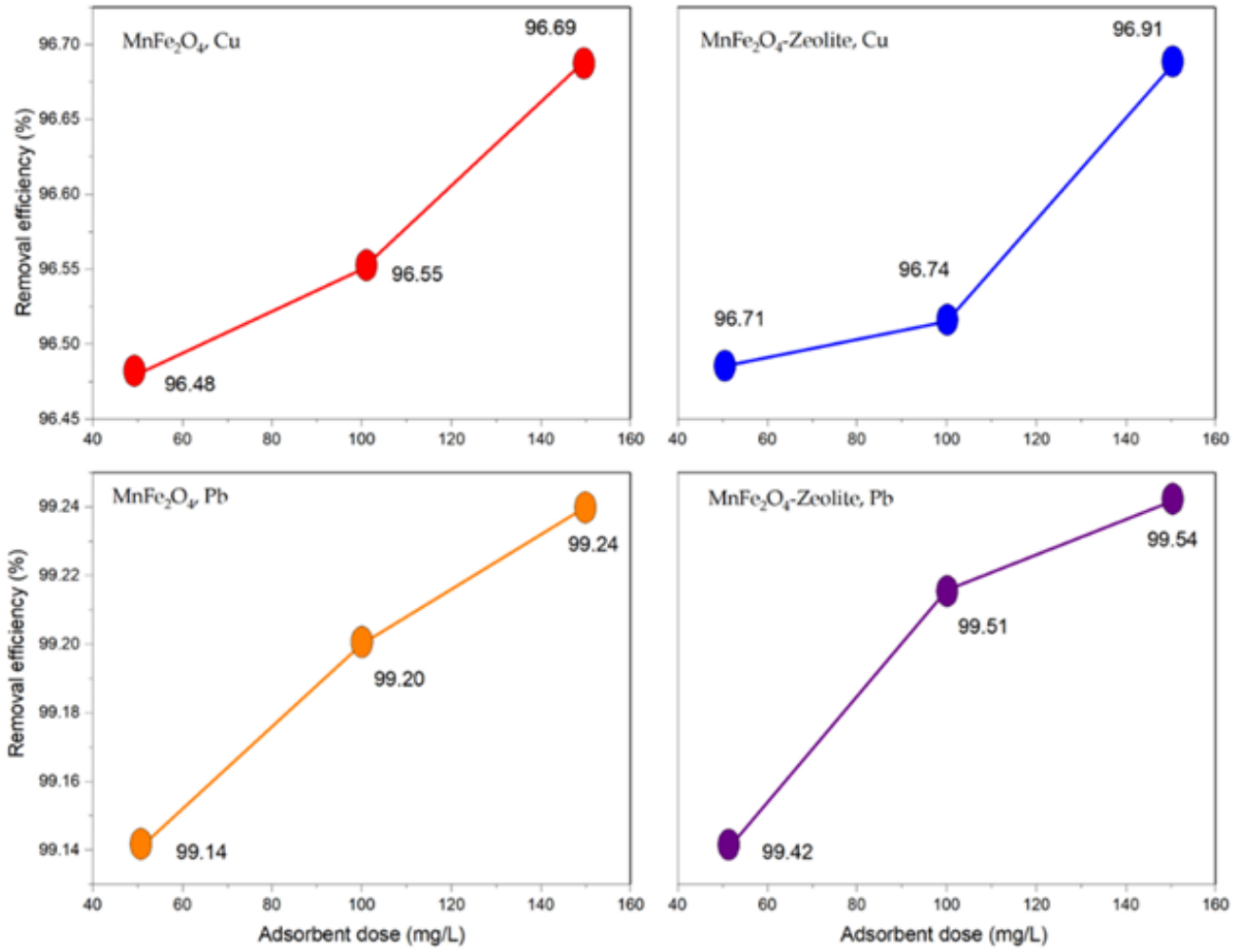

Figure 6. The removal efficiency of Pb(II) and Cu(II) metal ions for $MnFe_2O_4$ dan $MnFe_2O_4$-Zeolite adsorbents.

Figure 6, It can be seen that the removal efficiency of Cu(II) ions using both $MnFe_2O_4$ and $MnFe_2O_4$ -Zeolite adsorbents is higher than the removal efficiency of Pb(II) ions. This is due to the smaller radius of Cu(II) ions (0.72 Å) compared to Pb(II) (1.29 Å) so that Cu(II) metal ions can easily occupy the adsorption active sites on the adsorbent surface [31][32]. The removal efficiency value is also increased when the adsorbent dose increases from 50, 100, and 150 mg/L. By increasing the adsorbent dose, the number of active sites is also increased. Then particle aggregation will occur, which makes the adsorption efficiency of Pb and Cu increase.

The removal efficiency is also influenced by the use of adsorbent pH, where if the pH used is more than 6, Pb(II) ions will precipitate in the form of hydroxide $Pb(OH)_2$, which will reduce the concentration of Pb ions in the solution and then decrease the removal efficiency [1]. The presence of hydrogen ions (H+) from the deprotonation of hydroxyl groups in water also affects the removal efficiency, where H+ ions will compete with Pb(II) and Cu(II) ions to occupy active sites on the adsorbent [33].

The removal efficiency of Pb and Cu ions using $MnFe_2O_4$-zeolite is higher than $MnFe_2O_4$ adsorbent, which is also due to the addition of zeolite increases the surface area, thus increasing the number of adsorption active sites on the adsorbent surface [32], and also with the presence of Na+ cations from zeolite analcime can be exchanged with Pb^{2+} (1.29A) or Cu^{2+} (0.72A) cations [34][35]. Where the radius of Na ions is 1.02 Å, the addition of zeolite increases the surface area and increases the number of active adsorption sites on the surface of the adsorbent, thereby increasing the adsorption capacity.

In Table 2, the comparison of adsorption capacity with various adsorbents for Pb(II), and Cu(II). As can be seen from Table 2, the adsorption capacity of Pb and Cu by several researchers using different samples. For example, in sample CG, batch mode adsorption studies of Cu(II), Ni(II), Pb(II), and Co(II) were conducted at 25°C using 200 ml of metal ion solutions with concentrations ranging from 10-50 mg/L and 400 mg of adsorbent with an adsorption capacity of 16.95 mg/g for Pb metal and 6.64 mg/g for Cu metal [44]. Compared to the results of our research which was also conducted at 25°C using a 1L water solution has a fairly good adsorption capacity for $MnFe_2O_4$ absorbent of 7.72 mg/g for Pb metal and 7.94 mg/g for Cu metal. While $MnFe_2O_4$-Zeolite absorbent has an absorption capacity of 7.74 mg/g for Pb metal and 7.96 mg/g for Cu metal. The amount of both absorbents was 150 mg, and the initial concentration of Pb and Cu metal was 8 mg/L as seen in Table 1. We didn't do the variation concentration in this work due to the limitations of the samples of Pb and Cu Metals.

Table 2. The comparison of adsorption capacity with various adsorbents for Pb(II) and Cu(II).

No	Sample	Ads. capacity (mg g^{-1})		Ref
		Pb	Cu	
1	chitosan/graphene oxide composites	76.9		[45]
2	GO	328		[46]
3	EDTA−GO	479		[46]
4	EDTA−RGO	204		[46]
5	amino-functionalized carbon nanotubes	58.3		[47]
8	Fe_3O_4/Cu-MOFs	219.00		[49]
9	ZnO/MMT	88.50	54.06	[50]
10	CG	16.95	6.64	[51]
11	CG-0.5GEC	16.95	7.91	[51]
12	CG-1.0GEC	17.01	7.54	[51]
13	CG-2.0GEC	17.70	8.64	[51]
14	CMS@CS		63.7	[52]
15	CMS@CS-F		66.7	[52]
16	PANI@APTS-Fe_3O_4/ATP-0.7 (288K)	265.25	180.18	[53]
17	PANI@APTS-Fe_3O_4/ATP-0.7 (298K)	270.27	189.03	[53]
18	PANI@APTS-Fe_3O_4/ATP-0.7 (308K)	273.22	198.80	[53]
19	EDTA-mGO (298K)	481.2	246.1	[54]
20	EDTA-mGO (308K)	548.1	289.4	[54]
21	EDTA-mGO (318K)	508.4	301.2	[54]
22	chitosan-pyromellitic dianhydride		66.7432	[55]
23	CFZ10-68	109.890	57.803	[56]
24	ZRef – FAU	103.093	57.803	[56]
25	Oxidized MWCNT/SDBS	66.95		[57]
26	Oxidized MWCNT	17.5		[58]
27	Activated carbon/zeolite	549.11		[59]
28	$MnFe_2O_4$	7.72	7.94	This work
29	$MnFe_2O_4$ – Zeolite	7.74	7.96	This work

4. CONCLUSION

In this study, $MnFe_2O_4$ and $MnFe_2O_4$–zeolite were successfully synthesized from sand and zeolite using the Co-precipitation method for use as adsorbents for the adsorption of Pb(II) and Cu(II) ions from aqueous media. The results of the SEM-EDX analysis showed that the $MnFe_2O_4$ and $MnFe_2O_4$–zeolite particles had non-uniform particle sizes with some impurities present. XRD analysis confirmed the presence of impurities with the appearance of TiO_2 and SiO_2 peaks. Both adsorbents are ferrimagnetic and show soft magnet behavior, with the coercivity value of $MnFe_2O_4$–zeolite being larger than that of $MnFe_2O_4$. The BET analysis also showed that the surface area, pore volume, and pore size of the $MnFe_2O_4$-zeolite adsorbent are larger than those of the $MnFe_2O_4$ adsorbents. From the adsorption test with the influence of the adsorbent dose, there was an increase in the percentage of optimum adsorption on Pb and Cu by using the $MnFe_2O_4$-zeolite adsorbent. From this study, it was found that $MnFe_2O_4$-zeolite is a very effective sorbent in removing Cu and Pb ions from aqueous solution. This is because it has a good absorption capacity, which is above (>95%) for each heavy metal, and increased absorption after compositing with zeolite.

ACKNOWLEDGMENTS

The research/publication of this article was a collaboration between the National Research and Innovation Agency (BRIN) and Universitas Sriwijaya, and part is funded by DIPA of Public Service Agency of Universitas Sriwijaya 2023. Nomor SP DIPA-023.17.2.677515/2023, On November 30, 2022. By the Rector's Decree Number: 0188/UN9.3.1/SK/2023, On April 18, 2023.

REFERENCES

[1] Hassan M R, Aly M I. Magnetically Synthesized MnFe2O4 Nanoparticles as an Effective Adsorbent for Lead Ions Removal from an Aqueous Solution. *Aqua Water Infrastructure, Ecosyst. Soc*. 2021;70(6):901-920. doi:10.2166/aqua.2021.132.

[2] Bhateria R, Singh R. A Review on Nanotechnological Application of Magnetic Iron Oxides for Heavy Metal Re-

moval. *J. Water Process Eng*. 2019;31(October 2018):100845. doi:10.1016/j.jwpe.2019.100845.

[3] Bonyadi Z. Ultrasonic-assisted synthesis of Populus alba activated carbon for water defluorination: Application for real wastewater. *Korean J. Chem. Eng*. 2019;36(10):1595-1603. doi:10.1007/s11814-019-0373-0.

[4] Zare E N, Motahari A, Sillanpää M. Nanoadsorbents Based on Conducting Polymer Nanocomposites with Main Focus on Polyaniline and its Derivatives for Removal of Heavy Metal Ions/Dyes: A Review. *Environ. Res*. 2018;162:173-195. doi:10.1016/j.envres.2017.12.025.

[5] Ramlan Ramlan, Melinia Luh Ayu, Naibaho Marzuki, Puspita Endah, Ginting Masno. Review on The Adsorption of Heavy Metals in Water by MnFe2O4 and Zeolite. *Indones. Phys. Rev*. 2024;6(2):196-219. doi:10.29303/ip.

[6] Ghezelbash S, Yousefi M, Hossainisadr M, Baghshahi S. Structural and Magnetic Properties of Sn4+ Doped Strontium Hexaferrites Prepared via Sol–Gel Auto-Combustion Method. *IEEE Trans. Magn*. 2018:1-6. doi:10.1109/TMAG.2018.2844364.

[7] Thaçi B S, Gashi S T. Reverse Osmosis Removal of Heavy Metals from Wastewater Effluents Using Biowaste Materials Pretreatment. *Polish J. Environ. Stud*. 2019;28(1):337-341. doi:10.15244/pjoes/81268.

[8] Dong L, Hou L, Wang Z, Gu P, Chen G, Jiang R. A New Function of Spent Activated Carbon in BAC Process: Removing Heavy Metals by Ion Exchange Mechanism. *J. Hazard. Mater*. 2018;359:76-84. doi:10.1016/j.jhazmat.2018.07.030.

[9] Zhang Y, Duan X. Chemical Precipitation of Heavy Metals from Wastewater by Using the Synthetical Magnesium Hydroxy Carbonate. *Water Sci. Technol*. 2020;81(6):1130-1136. doi:10.2166/wst.2020.208.

[10] Shih Y J, Chien S K, Jhang S R, Lin Y C. Chemical Leaching, Precipitation and Solvent Extraction for Sequential Separation of Valuable Metals in Cathode Material of Spent Lithium Ion Batteries. *J. Taiwan Inst. Chem. Eng*. 2019;100:151-159. doi:10.1016/j.jtice.2019.04.017.

[11] doi:10.1016/j.jcis.2016.11.098.

[12] Esmaeili H, Foroutan R. Adsorptive Behavior of Methylene Blue onto Sawdust of Sour Lemon, Date Palm, and Eucalyptus as Agricultural Wastes. *J. Dispers. Sci. Technol*. 2019;40(7):990-999. doi:10.1080/01932691.2018.1489828.

[13] Joya M Rincón, Ortega J Barba, Malafatti J O D, Paris E C. Evaluation of Photocatalytic Activity in Water Pollutants and Cytotoxic Response of α-Fe2O3 Nanoparticles. *ACS Omega*. 2019;4(17):17477-17486. doi:10.1021/acsomega.9b02251.

[14] Ramlan Ramlan, Bama A A, Johan A, Naibaho M, Ginting M. Synthesis and Characterization of Hematite (α-Fe2O3) from Iron Sand Using Coprecipitation Method. *Key Eng. Mater*. 2024;985:145-151. doi:10.4028/p-uib7jj.

[15] Novita N, Ramlan Ramlan, Naibaho M, Ginting M, Humaidi S, Duma T N. Fe2O3 Review: Nanostructure, Synthesis Methods, and Applications. *Int. J. Soc. Serv. Res*. 2024;4(02):539-559. doi:10.46799/ijssr.v4i02.728.

[16] Elysia Z, Naibaho M, Faye H, Huang T. The impact of hydrolysis process on the performance of polyacrylonitrile membrane in the separation of dye substances. 2025;9(September).

[17] Naibaho M, Fauzi N, Puspita E, Bama A A, Ramlan Ramlan, Indayaningsih N. Pembuatan Karbon Serat Sabut Kelapa dan Pengujian Konduktivitas Listriknya. *J. Penelit. Sains*. 2022;24(2):64. doi:10.56064/jps.v24i2.690.

[18] Jo J Y, Choi J H, Tsang Y F, Baek K. Pelletized Adsorbent of Alum Sludge and Bentonite for Removal of Arsenic. *Environ. Pollut*. 2021;277:116747. doi:10.1016/j.envpol.2021.116747.

[19] Kobayashi Y, Ogata F, Nakamura T, Kawasaki N. Synthesis of Novel Zeolites Produced from fly Ash by Hydrothermal Treatment in Alkaline Solution and its Evaluation as an Adsorbent for Heavy Metal Removal. *J. Environ. Chem. Eng*. 2020;8(2):103687. doi:10.1016/j.jece.2020.103687.

[20] Puspita E, Naibaho M, Ramlan Ramlan, Ginting M. Morphologycal, Elemental Content, and Physical Properties of Cleaned Clinoptitolite Zeolite (10X) Using Sonication and Microwave. *Indones. Phys. Rev*. 2023;6(1):95-104. doi:10.29303/ipr.v6i1.204.

[21] Martinez–Vargas S. As(III) and As(V) Adsorption on Manganese Ferrite Nanoparticles. *J. Mol. Struct*. 2018;1154(Iii):524-534. doi:10.1016/j.molstruc.2017.10.076.

[22] Fajaroh F, Susilowati I D, Nazriati, Sumari, Nur A. Synthesis of ZnFe2O4 Nanoparticles with PEG 6000 and Their Potential Application for Adsorbent. *IOP Conf. Ser. Mater. Sci. Eng*. 2019;515(1):1-9. doi:10.1088/1757-899X/515/1/012049.

[23] Xu Z. Manganese Ferrite Modified Biochar from Vinasse for Enhanced Adsorption of Levofloxacin: Effects and Mechanisms. *Environ. Pollut*. 2021;272:115968. doi:10.1016/j.envpol.2020.115968.

[24] Ahmadi A, Foroutan R, Esmaeili H, Tamjidi S. The role of bentonite clay and bentonite clay@MnFe2O4 composite and their physico-chemical properties on the removal of Cr(III) and Cr(VI) from aqueous media. *Environ. Sci. Pollut. Res*. 2020;27(12):14044-14057. doi:10.1007/s11356-020-07756-x.

[25] Wang R, Liang R, Dai T, Chen J, Shuai X, Liu C. Pectin-Based Adsorbents for Heavy Metal Ions: A Review. *Trends Food Sci. Technol*. 2019;91(May 2018):319-329. doi:10.1016/j.tifs.2019.07.033.

[26] Akhlaghi N, Najafpour-Darzi G. Manganese Ferrite (MnFe2O4) Nanoparticles: From Synthesis to Application -A Review. *J. Ind. Eng. Chem*. 2021;103:292-304. doi:10.1016/j.jiec.2021.07.043.

[27] Amrollahi A, Massinaei M, Moghaddam A Z. Removal of the residual xanthate from flotation plant tailings using bentonite modified by magnetic nano-particles. *Miner. Eng*. 2019;134(January):142-155. doi:10.1016/j.mineng.2019.01.031.

[28] Puspita Endah, Melinia Luh Ayu, Naibaho Marzuki, Ramlan Ramlan, Ginting dan Masno. Sintesis dan karakterisasi pasir besi Sungai Musi Sumatera Selatan menggunakan metode kopresipitasi Endah. *J. Penelit. Sains*. 2022;24(3):160-165.

[29] Melinia L A, Puspita E, Naibaho M, Ramlan Ramlan, Ginting M. Analisa Pasir Besi Alam dari Sungai Musi Sumatera Selatan. *J. Penelit. Sains*. 2022;24(3):122. doi:10.56064/jps.v24i3.716.

[30] Novita N, Naibaho M, Puspita E, Ramlan Ramlan, Ginting M, Humaidi S. Analysis of Mineral Content and Magnetic Properties of Iron Sand of Bah Bolon Simalungun River, North Sumetera. *Asian J. Eng. Soc. Heal*. 2023;2(12):1633-1639. doi:10.46799/ajesh.v2i12.196.

[31] Puspita E, Ginting M, Ramlan Ramlan. Preparation and Characterization of Fe2O3 from Iron Sand of the Coastal Sea of Cidaun Beach-South Cianjur (Indonesia) using the Coprecipitation Method. *Sci. Technol. Indones*. 2023;8(4):594-598. doi:10.26554/sti.2023.8.4.594-598.

[32] Zhao Y, Li Q, Ren H, Zhou R. Activation of persulfate by magnetic MnFe2O4-bentonite for catalytic degradation of 2,4-dichlorophenol in aqueous solutions. *Chem. Res. Chinese Univ*. 2017;33(3):415-421. doi:10.1007/s40242-017-6485-3.

[33] Amulya M A S, Nagaswarupa H P, Kumar M R A, Ravikumar C R, Kusuma K B. Sonochemical Synthesis of MnFe2O4 Nanoparticles and their Electrochemical and Photocatalytic Properties. *J. Phys. Chem. Solids*. 2021;148(August 2020):109661. doi:10.1016/j.jpcs.2020.109661.

[34] Mondal D K, Borgohain C, Paul N, Borah J P. Tuning hyperthermia efficiency of MnFe2O4/ZnS nanocomposites by controlled ZnS concentration. *J. Mater. Res. Technol*. 2019;8(6):5659-5670. doi:10.1016/j.jmrt.2019.09.034.

[35] Novembre D, Gimeno D. Synthesis and Characterization of Analcime (ANA) Zeolite using a Kaolinitic rock. *Sci. Rep*. 2021;11(1):1-9. doi:10.1038/s41598-021-92862-0.

[36] Bortolini H R, Lima D S, Perez-Lopez O W. Hydrothermal synthesis of analcime without template. *J. Cryst. Growth*. 2020;532(November 2019):125424. doi:10.1016/j.jcrysgro.2019.125424.

[37] doi:10.3390/inorganics8010006.

[38] Gautam S. Superparamagnetic MnFe2O4 Dispersed Over Graphitic Carbon Sand Composite and Bentonite as Magnetically Recoverable Photocatalyst for Antibiotic Mineralization. *Sep. Purif. Technol*. 2017;172:498-511.

doi:10.1016/j.seppur.2016.09.006.

[39] Zheng M, Wu X C, Zou B S, Wang Y J. Magnetic properties of nanosized MnFe2O4 particles. *J. Magn. Magn. Mater*. 1998;183(1–2):152-156. doi:10.1016/S0304-8853(97)01057-3.

[40] Barsotti E, Tan S P, Piri M, Chen J H. Capillary-condensation hysteresis in naturally-occurring nanoporous media. *Fuel*. 2020;263(August):116441. doi:10.1016/j.fuel.2019.116441.

[41] Bardestani R, Patience G S, Kaliaguine S. Experimental methods in chemical engineering: specific surface area and pore size distribution measurements—BET, BJH, and DFT. *Can. J. Chem. Eng*. 2019;97(11):2781-2791. doi:10.1002/cjce.23632.

[42] Duan H, Hu X, Sun Z. Magnetic zeolite imidazole framework material-8 as an effective and recyclable adsorbent for removal of ceftazidime from aqueous solution. *J. Hazard. Mater*. 2020;384(October 2019):121406. doi:10.1016/j.jhazmat.2019.121406.

[43] Wang F Y, Wang H, Ma J W. Adsorption of cadmium (II) ions from aqueous solution by a new low-cost adsorbent-Bamboo charcoal. *J. Hazard. Mater*. 2010;177(1–3):300-306. doi:10.1016/j.jhazmat.2009.12.032.

[44] Alghamdi A A, Al-Odayni A B, Saeed W S, Al-Kahtani A, Al-harthi F A, Aouak T. Efficient adsorption of lead (II) from aqueous phase solutions using polypyrrole-based activated carbon. *Materials (Basel)*. 2019;12(12). doi:10.3390/ma12122020.

[45] Fan L, Luo C, Sun M, Li X, Qiu H. Highly selective adsorption of lead ions by water-dispersible magnetic chitosan/graphene oxide composites. *Colloids Surfaces B Biointerfaces*. 2013;103:523-529. doi:10.1016/j.colsurfb.2012.11.006.

[46] Madadrang C J. Adsorption behavior of EDTA-graphene oxide for Pb (II) removal. *ACS Appl. Mater. Interfaces*. 2012;4(3):1186-1193. doi:10.1021/am201645g.

[47] Vuković G D. Removal of lead from water by amino modified multi-walled carbon nanotubes. *Chem. Eng. J*. 2011;173(3):855-865. doi:10.1016/j.cej.2011.08.036.

[48] Shi Z. Magnetic metal organic frameworks (MOFs) composite for removal of lead and malachite green in wastewater. *Colloids Surfaces A Physicochem. Eng. Asp*. 2018;539(2010):382-390. doi:10.1016/j.colsurfa.2017.12.043.

[49] Sani H A, Ahmad M B, Hussein M Z, Ibrahim N A, Musa A, Saleh T A. Nanocomposite of ZnO with montmorillonite for removal of lead and copper ions from aqueous solutions. *Process Saf. Environ. Prot*. 2017;109:97-105. doi:10.1016/j.psep.2017.03.024.

[50] Osińska M. Removal of lead(II), copper(II), cobalt(II) and nickel(II) ions from aqueous solutions using carbon gels. *J. Sol-Gel Sci. Technol*. 2017;81(3):678-692. doi:10.1007/s10971-016-4256-0.

[51] Zhang L T. Low-Cost magnetic adsorbent for efficient Cu(II) removal from water. *Mater. Res. Express*. 2020;7(10). doi:10.1088/2053-1591/abbe3f.

[52] Sun P, Zhang W, Zou B, Wang X, Zhou L, Ye Z. Applied Clay Science Efficient adsorption of Cu (II), Pb (II) and Ni (II) from waste water by PANI @ APTS-magnetic attapulgite composites. 2021;209(January).

[53] Cui L. EDTA functionalized magnetic graphene oxide for removal of Pb(II), Hg(II) and Cu(II) in water treatment: Adsorption mechanism and separation property. *Chem. Eng. J*. 2015;281:1-10. doi:10.1016/j.cej.2015.06.043.

[54] Deng J. Competitive adsorption of Pb(II), Cd(II) and Cu(II) onto chitosan-pyromellitic dianhydride modified biochar. *J. Colloid Interface Sci*. 2017;506:355-364. doi:10.1016/j.jcis.2017.07.069.

[55] Joseph I V, Tosheva L, Doyle A M. Simultaneous removal of Cd(II), Co(II), Cu(II), Pb(II), and Zn(II) ions from aqueous solutions via adsorption on FAU-type zeolites prepared from coal fly ash. *J. Environ. Chem. Eng*. 2020;8(4):103895. doi:10.1016/j.jece.2020.103895.

[56] Li J, Chen S, Sheng G, Hu J, Tan X, Wang X. Effect of surfactants on Pb(II) adsorption from aqueous solutions using oxidized multiwall carbon nanotubes. *Chem. Eng. J*. 2011;166(2):551-558. doi:10.1016/j.cej.2010.11.018.

[57] Ren X. Comparative study of Pb(II) sorption on XC-72 carbon and multi-walled carbon nanotubes from aqueous solutions. *Chem. Eng. J*. 2011;170(1):170-177. doi:10.1016/j.cej.2011.03.050.

[58] Jha V K, Matsuda M, Miyake M. Sorption properties of the activated carbon-zeolite composite prepared from coal fly ash for Ni2+, Cu2+, Cd2+ and Pb2+. *J. Hazard. Mater*. 2008;160(1):148-153. doi:10.1016/j.jhazmat.2008.02.107.

